Journal of Vinyl and Additive Technology

WILEY | spe INSPIRING PLASTICS PROFESSIONALS

RESEARCH ARTICLE OPEN ACCESS

Development of Polyurethane-Based Composites With Salt Clay and Industrial Wastes as Fillers: Corrosion, Mechanical Properties, and Machine Learning Insights

Mustafa Dağ[1] | Ercan Aydoğmuş[2] | Hasan Arslanoğlu[3] | Zehra Gülten Yalçin[1] | Semahat Barlak[1]

[1]Engineering Faculty, Chemical Engineering, Çankırı Karatekin University, Çankırı, Türkiye | [2]Engineering Faculty, Chemical Engineering, Fırat University, Elâzığ, Türkiye | [3]Engineering Faculty, Chemical Engineering, Çanakkale Onsekiz Mart University, Çanakkale, Türkiye

Correspondence: Hasan Arslanoğlu (hasan.arslanoglu@comu.edu.tr)

Received: 5 March 2025 | **Revised:** 6 May 2025 | **Accepted:** 11 May 2025

Funding: This work was supported by Fırat University Scientific Research Projects Unit [ADEP.25.07].

Keywords: industrial wastes | insulation material | machine learning | polyurethane-based composites | salt clay

ABSTRACT

In this study, a polyurethane-based composite is developed by incorporating salt clay, ulexite, colemanite, and various other industrial waste materials. The effects of these fillers on the composite are evaluated and modeled using machine learning techniques. Among the tested models, random forest and neural network demonstrate the highest performance in predicting changes in compressive strength, hardness, and thermal conductivity. The dispersion of salt clay within the polyurethane matrix provides a 300%–500% increase in compressive strength and a 25%–40% improvement in hardness. Ulexite enhances compressive strength by 250%–350% and increases hardness by up to 30%, while colemanite contributes to a 400%–500% rise in compressive strength and a 35%–40% improvement in hardness. The addition of Kırka clay waste and tincal further improves the composite's hardness and overall durability. Fly ash significantly increases compressive strength, although its effect on hardness is limited. The machine learning models effectively capture the relationship between input parameters and composite performance. The random forest model achieves a mean squared error (MSE) of 0.15 for compressive strength and 0.20 for hardness, while the neural network model yields the best results for thermal conductivity prediction with an MSE of 0.12. These findings highlight the potential of the developed composite for industrial applications, particularly in thermal insulation and low-load structural components. Future studies will focus on evaluating its performance under real-world conditions and further assessing its long-term durability.

1 | Introduction

In a globalized world, the struggle for economic power has made competition in production and technology inevitable. This competition has led to the depletion of natural resources and increased pollution [1–3]. Aware of the negative consequences of pollution and waste, scientists have initiated studies on waste management and recovery. These wastes typically originate from industrialization, overuse of natural resources, air pollution, agricultural chemicals, and waste accumulation. Methods for waste disposal include recycling [4, 5], utilizing waste as raw materials in various processes, and incineration. However, it is essential to dispose of waste without harming nature and human health. In response to the rapidly increasing volume of waste during the industrialization process [6–8], waste management practices have been revised in line with the zero-waste principle. Instead of direct disposal, recycling and recovery processes have gained importance. Regulations have been implemented to manage different types of waste, such as batteries and accumulators,

Summary

- Industrial Wastes in Polymer Composites were developed as green thermal insulators.
- Machine Learning treatment on clean, environmentally friendly heat insulator composites was applied.
- The treatments significantly improved the mechanical properties of composites.
- The treated composites maintained high thermal insulation properties.

industrial waste [9], medical waste, clamshell waste [10], hazardous waste, sludge [11, 12], and construction and demolition debris. These wastes are incorporated into various materials as raw materials for disposal and reevaluation. In this context, composite materials serve both as valuable materials for the future and as a means of utilizing waste. Composite materials [13–16] are defined as innovative materials formed by combining two or more different components, each offering its best properties. Historically used in the form of straw-based adobe, composite materials are now preferred when their enhanced properties are needed. These materials are noteworthy for their homogeneous microstructure and the preservation of the individual properties of the different components. Composites can be classified as fiber, particle, or layered composites based on the type of reinforcement element, and they can have metal, ceramic, or polymer matrices [17–20]. Composites offer several advantages, including high strength, lightweight, design flexibility, ease of shaping, electrical insulation, resistance to corrosion and chemical effects, and low cost [21–24]. However, composites also present challenges, such as susceptibility to air pockets, variability in mechanical properties, and the need for precise manufacturing techniques.

In this study, polyurethane was used as the matrix. Polyurethanes are polymers that can be produced with varying properties by altering the amounts of different silicones, catalysts, and blowing agents along with isocyanates and polyols. They can be categorized into various classes, including rigid, flexible, water-based, vegetable oil-based, adhesives, binders, coatings, sealants, and elastomers. The polyols used in polyurethane production [25–27] are oligomers in the liquid phase or polymeric compounds with two or more hydroxyl groups. Vegetable oil-based polyols [26, 28] hold significant importance in the polyurethane industry, with highly unsaturated oils being preferred. Clay [29–31] wastes were used as fillers in the production of the composites. These clay wastes are by-products obtained from the salt mines in Çankırı, released during the refining of rock salt. In the refining process, approximately 75% of the daily raw salt input is converted into refined salt, while the remaining 25% is released as clay waste.

Other fillers and industrial wastes used in this study include ulexite, colemanite, Kırka clay waste, tincal, coal ash (fly ash), ulexite clay (70% water), and colemanite clay (70% water). Each filler and waste material was selected with the goal of imparting specific properties to the composite. In this context, salt clay waste was used as the reference material, with the objective of enhancing the properties of the composite and either reinforcing these properties or introducing new functionalities through additional fillers. Literature reviews indicate that various studies have utilized ulexite [32], colemanite [33, 34] Kırka clay waste, tincal, coal ash [35] (fly ash), ulexite clay (70% water), and colemanite clay (70% water) as fillers and industrial wastes. Inspired by these studies, different approaches were tested, and these experiments were modeled using machine learning techniques. In recent years, machine learning methods have been increasingly utilized to predict and optimize the performance of such composite materials [36–38]. Similarly, machine learning allows us to understand the effects of complex material compositions on mechanical and corrosion properties and to capture nonlinear relationships; in the literature, the effective thermal conductivity of polymer composites reinforced with spherical filler particles has been modeled using the finite element method [39], demonstrating that models developed via diverse analytical and numerical approaches can produce complementary and correlated results. Models such as random forest [40–42] and artificial neural networks [16, 43] have been particularly successful in accurately predicting the effects of fillers on the properties of polyurethane composites [27, 44–46]. These approaches accelerate the material development process while also providing cost and resource savings, which is one of the aims of this study as well.

In this study, instead of employing traditional experimental design models, modeling was performed directly from the experimental results using machine learning. The industrial applicability of the obtained results was investigated. Within this scope, a polyurethane-based composite was produced using a polyol matrix, primarily with salt clay waste as a fundamental filler, along with other industrial wastes. The physical and chemical properties of the resulting polyurethane-based composite were investigated, and the analysis results were modeled using machine learning. The potential applications of the produced composite in various industrial fields were explored, and a roadmap for future studies was established.

2 | Materials and Methods

2.1 | Obtaining Polyurethane-Based Composites

In this investigation, the polymer matrix was prepared from technical-grade methylene diphenyl diisocyanate (MDI, NCO content 31%, Merck) and commercial polyol (CP, ≥ 99% purity, Sigma-Aldrich). The polyol was selected based on its molecular weight (2500–3000 g/mol), functional-group density, viscosity, and raw-material temperature—parameters shown to critically influence prepolymer formation. A cobalt octoate catalyst (5 wt.% Co Oc, Strem Chemicals) was added to accelerate urethane linkage development, while industrial salt-clay waste (dried at 105 C, milled to ≤ 50 μm) served as both filler and additive, improving nucleation and thermal performance. Stoichiometric ratios of polyol to MDI were calculated at 25 °C using a 100 g polyol basis; thereafter, the required amounts of MDI, cobalt catalyst, salt-clay filler, and any additional industrial-waste fillers were determined to produce the final polyurethane composite. The composition of the additives used in the experimental studies is as follows: salt

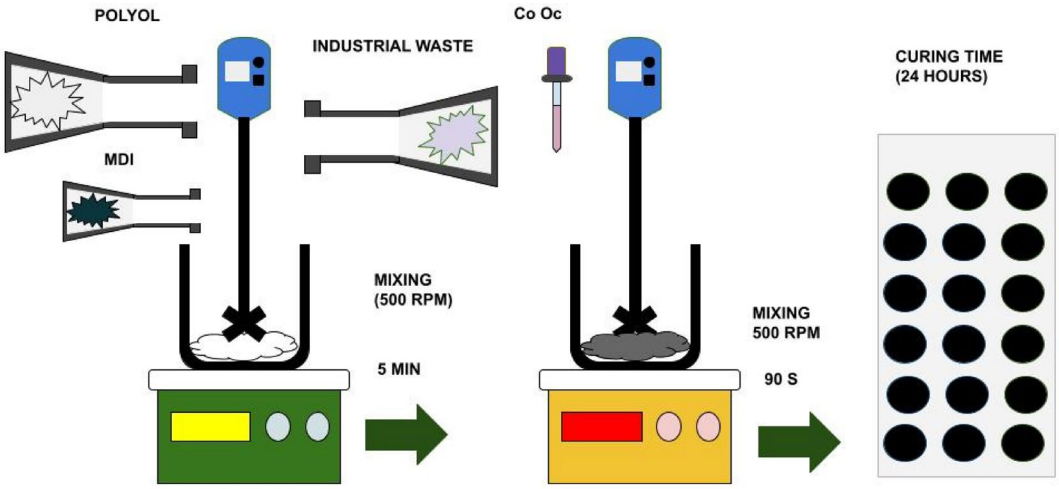

FIGURE 1 | A schematic experimental diagram.

TABLE 1 | Types of wastes used in composites.

Waste no.	Type of waste
1	Salt clay waste
2	Ulexite
3	Colemanite
4	Kırka clay waste
5	Tincal
6	Coal ash (fly ash)
7	Ulexite clay (70 wt.% water)
8	Colemanite clay (70 wt.% water)

clay waste consists of sodium chloride (NaCl), sodium sulfate (Na_2SO_4), magnesium chloride ($MgCl_2$), magnesium sulfate ($MgSO_4$), and their hydrated forms, with minor amounts of calcium and potassium salts. The chemical formula of ulexite is $NaCaB_5O_9{\cdot}8H_2O$; it contains sodium borate ($Na_2B_4O_7$), calcium borate ($CaB_3O_4(OH)_3{\cdot}H_2O$), and eight molecules of crystal water. Colemanite is $Ca_2B_6O_{11}{\cdot}5H_2O$, comprising calcium borate ($CaB_3O_4(OH)_3$) and five bound water molecules. Kırka clay waste typically contains approximately $Al_2Si_2O_5(OH)_4$ (kaolinite), 1%–5% $CaCO_3$ (calcite), $MgCO_3$ (magnesite), plus fine silica (SiO_2), and trace Fe_2O_3. Tincal (borax) is $Na_2B_4O_7{\cdot}10H_2O$, consisting of sodium borate ($Na_2B_4O_7$) and ten molecules of crystal water. Coal ash (fly ash) contains roughly 50%–60% SiO_2, 20%–30% Al_2O_3, 5%–10% Fe_2O_3, 1%–5% CaO, along with MgO, K_2O, Na_2O, and trace TiO_2, SO_3. Ulexite clay (70% water) carries the base ulexite composition ($NaCaB_5O_9$) plus 70% H_2O. Colemanite clay (70% water) contains the base colemanite composition ($Ca_2B_6O_{11}$) with its five bound water molecules and a total of 70% H_2O.

Experimental studies were conducted with a systematic approach, involving the creation of a suspension by adding the filler in specific proportions and ensuring homogeneity in the experimental setup. A schematic diagram of the experiment is shown in Figure 1.

In this investigation, specific parameters were designated to maintain consistency, with a temperature of 25°C, a mixing speed set at 500 rpm, and a reaction time spanning 30 s to 15 min. Meanwhile, the mixing ratios of waste and the quantity of polymer were identified as variable parameters, allowing for a comprehensive exploration of their impact on the resulting composite.

The ensuing polymeric composite products underwent a range of analyses, including strength endurance tests (compressive strength), electrical conductivity determination, thermal conductivity determination, hardness determination, corrosion resistance assessment, Fourier-transform infrared spectroscopy (FTIR), scanning electron microscopy (SEM) analysis, and surface area determination. The obtained polymeric composite materials were coded as "o," "i," and "m." The pure polymer and waste materials used in the production of the composites, as well as the compositions of the composites, are provided in Tables 1, 2, respectively. The results of the analyses conducted on the produced composites are presented in Table 3.

2.2 | Shore A Hardness and Thermal Conductivity Tests of Polyurethane-Based Composites

Another important parameter for the obtained composite materials is their hardness. The hardness of the composite was determined using the Loyka LXA Shore A Hardness Tester. The accepted hardness values were obtained by averaging measurements taken from different points on each sample. The hardness measurement results of the samples are presented in Table 3.

Given that the obtained hard polyurethane foam composites find application in the insulation sector, an essential property sought in these materials is the thermal conductivity coefficient. The thermal conductivity in foam materials is contingent on factors such as foam density, cell size, the gas within the cell, and the properties of the polymer and fillers. Measurements of the thermal conduction coefficient were conducted using the TLS-100 measuring device, aligning with ASTM C1113 standards (specimens were cylindrical with a diameter of 50 mm and a thickness of 25 mm).

TABLE 2 | Composition of polymeric composite materials.

Sample code	Type of waste used	Polymer amount (g)	Waste amount (g)
1o	—	75	0
1i	1	50	25
9i	1-2	50	12.5-12.5
13i	1-2-3	50	8.25-8.25-8.25
15i	1-2-3-4	50	6.25-6.25-6.25-6.25
16i	1-2-3-4-5	50	5-5-5-5-5
17i	1-2-3-4-5-6	50	4.12-4.12-4.12-4.12-4.12-4.12
18i	1-2-3-4-5-6-7	50	3.5-3.5-3.5-3.5-3.5-3.5-3.5
19i	1-2-3-4-5-6-7-8	50	3.1-3.1-3.1-3.1-3.1-3.1-3.1-3.1
1 m	1	25	50
9 m	1-2	25	25-25
13 m	1-2-3	25	16.5-16.5-16.5
15 m	1-2-3-4	25	12.5-12.5-12.5-125
16 m	1-2-3-4-5	25	10-10-10-10-10
17 m	1-2-3-4-5-6	25	8.25-8.25-8.25-8.25-8.25-8.25
18 m	1-2-3-4-5-6-7	25	7-7-7-7-7-7-7
19 m	1-2-3-4-5-6-7-8	25	6.2-6.2-6.2-6.2-6.2-6.2-6.2-6.2

3 | Results and Discussion

In this study, it was observed that the thermal conductivity coefficients of the samples ranged between 0.030–0.050 W/m·K. The thermal conductivity coefficient of the pure commercial polyol was measured as 0.026 W/m·K, the hardness was measured as 67 Shore A, and the compressive strength was 0.13 MPa. Based on the thermal conductivity coefficient values, it can be concluded that all samples listed in Table 3 possess suitable values for use as insulation materials.

3.1 | Compressive Strength

Compressive strength tests, integral for assessing the physical characteristics of clay matrix-based composite materials, were conducted using computer-controlled BZ 001/60-OT-XC equipment with a capacity of 600 kN. The apparatus is illustrated in Figure 2, and the conducted tests adhered to the relevant American Society for Testing and Materials standards (ASTM 2010; specimens were cylindrical with a diameter of 50 mm and a thickness of 25 mm). Sample area values were input into the computer system, facilitating the determination of distortion points based on MPa and kN values. During the analyses, the compression process transpired at a speed of 0.2 kN/s perpendicular to the swelling direction of the composite materials. The pressing procedure persisted until the identification of the failure point, marked by the load drop and deformation depicted in the graph. The analysis results are presented in Table 3. Additionally, the compressive strength graphs of sample 1i and sample 1 m are shown in Figures 2 and 3, respectively.

As shown in Figure 2, the "1i" sample, with an area of 0.00636 m^2, exhibited resistance to a force of 6.248 kN and a compressive strength of 0.982 MPa.

As shown in Figure 3, the "1 m'" sample, with an area of 0.00640 m^2, exhibited resistance to a force of 8.621 kN and a compressive strength of 1.355 MPa.

3.2 | SEM Results

SEM is a technique that allows high-resolution imaging at large magnifications. With this technology, morphological, structural, and elemental information can be obtained at magnifications ranging from low scales to extremely high scales. In Figure 4, the SEM images of sample "1i" reveal that the mixture is not homogeneous in certain regions, with accumulation of fillers and additives observed in some areas. Additionally, particle sizes are seen to vary significantly. This can be interpreted as an indication of low-speed mixing during the preparation process. However, owing to the continuous structure of the mixture, only slight porosity is observed, as the gas-phase reaction proceeds in a uniform manner.

In Figure 5, the SEM image of sample "13i" shows that both mixing and the reaction were successfully completed, resulting in a composite with an almost smooth surface. The nearly uniform particle size of the fillers and the consistent mixing process contributed to this outcome. In sample "15i," despite the good dispersion, the differences in the particle sizes of the fillers, as well as inadequate mixing (leading to trapped residual gases), resulted in a composite with an irregular and porous structure. In sample "17 m," the uniform mixing of both fillers and fillers, along with consistent particle sizes, provided a smooth appearance, while the timely removal of residual gases prevented porosity formation.

3.3 | FTIR Spectra Results

In this study, molecular interactions and chemical characterizations were examined using an FTIR spectra. Figure 6 illustrates the FTIR spectrums of sample "1o." Key peaks and associated vibrational modes are as follows: 3297 cm^{-1} for N—H stretching vibrations, 2969 cm^{-1} for C—H asymmetric stretching vibrations, 2857 cm^{-1} for C-H symmetric stretching vibrations, 1740 cm^{-1} for C═O stretching vibrations, 1536 cm^{-1} for N-H bending vibrations, 1453 cm^{-1} for C—H shear vibrations, 1222 cm^{-1} for

TABLE 3 | Experimental results with standard deviations (Std. Dev.)

Sample no	Compressive strength (Max, MPa)	Std. Dev. (compressive strength)	Hardness (shore A)	Std. Dev. (hardness)	Thermal conductivity coefficient (W/m·K)	Std. Dev. (thermal conductivity)
1o	1.095	0.027	95	2.944	0.03	0.001
1i	0.982	0.047	90	2.455	0.032	0.001
9i	0.956	0.038	88	1.905	0.039	0.001
13i	0.753	0.026	82	2.827	0.041	0.001
15i	1.662	0.027	87	1.355	0.044	0.002
16i	0.333	0.005	90	1.952	0.037	0.001
17i	0.351	0.004	78	1.923	0.038	0.001
18i	0.40	0.018	87	2.457	0.052	0.002
19i	0.583	0.02	83	3.437	0.029	0.00
1 m	1.355	0.052	92	1.655	0.035	0.002
9 m	0.906	0.01	90	2.751	0.034	0.001
13 m	0.504	0.025	94	3.167	0.038	0.001
15 m	1.383	0.06	95	1.127	0.029	0.001
16 m	0.605	0.011	93	3.190	0.031	0.001
17 m	0.381	0.007	90	1.514	0.031	0.001
18 m	0.44	0.008	93	1.172	0.029	0.001
19 m	0.556	0.012	82	3.932	0.034	0.002

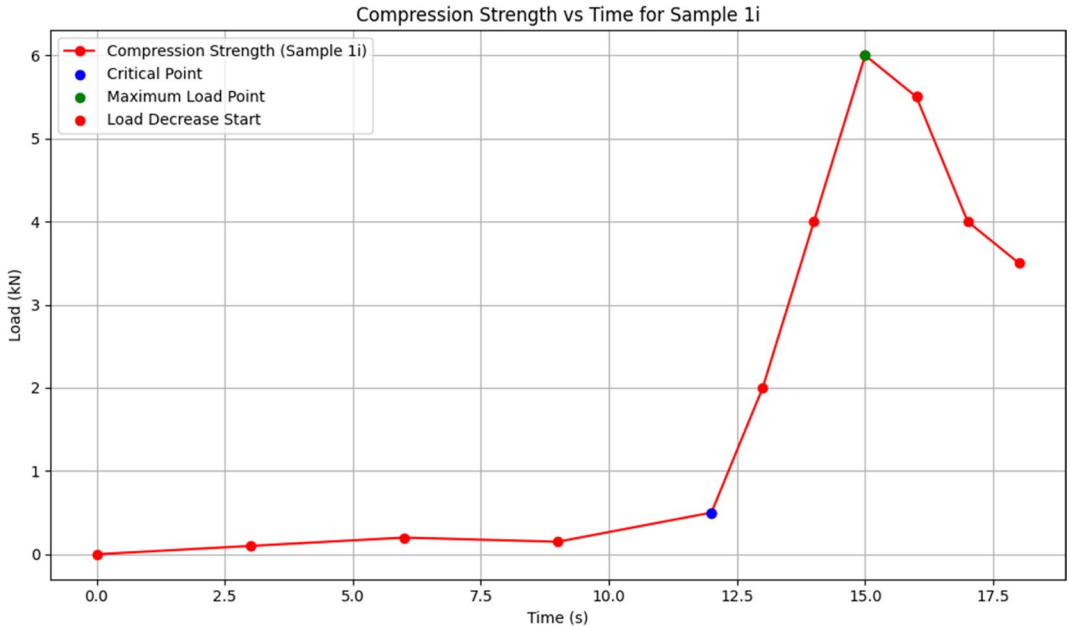

FIGURE 2 | Compression graph of polyurethane-based composite material with code "1i" under compressive load.

C—N stretching vibrations, and 1093 cm^{-1} for C—O stretching vibrations.

In Figure 7, the FTIR spectrums of sample "1i" is presented. A comparative analysis with the previous spectrums ("1o") suggests different interactions within the composite, evident in the band changes. Notably, specific vibrational modes and associated peaks include 1085 cm^{-1} for C—O stretching vibrations, 1230 cm^{-1} for C—N stretching vibrations, 1306 cm^{-1} for C—N (III) band stretching vibrations, 1508 cm^{-1} for aromatic C═C

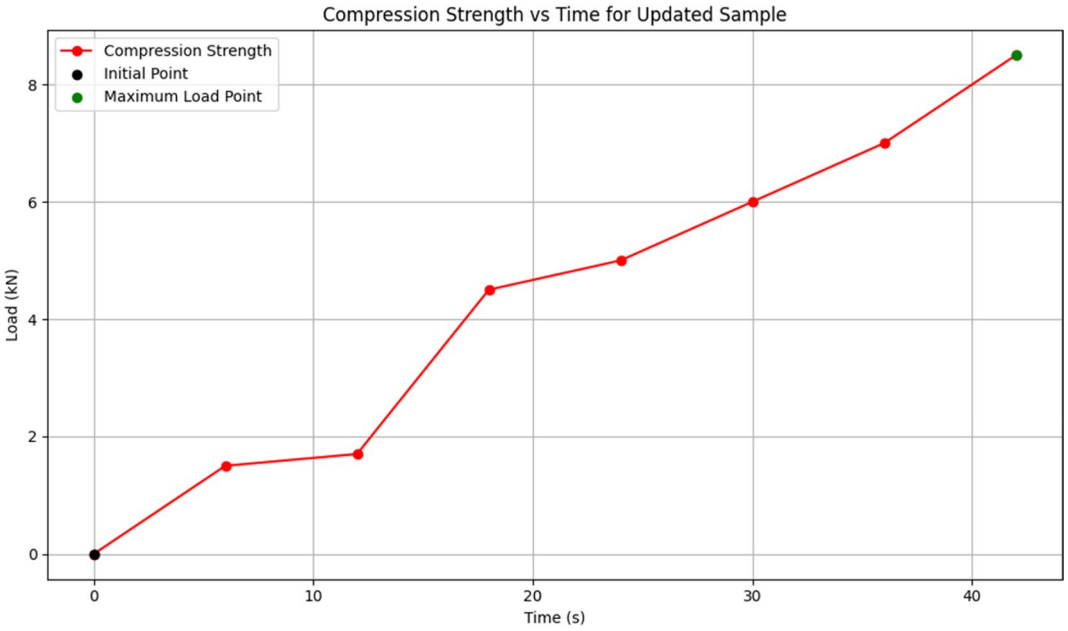

FIGURE 3 | Compression graph of polyurethane-based composite material with code "1 m" under compressive load.

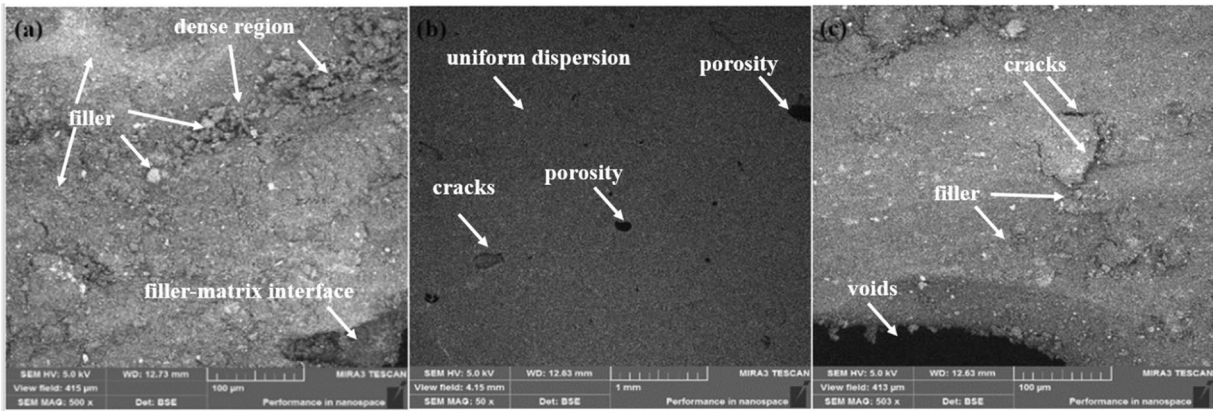

FIGURE 4 | SEM images of sample "1i": (a) interior, (b) exterior, (c) inner side.

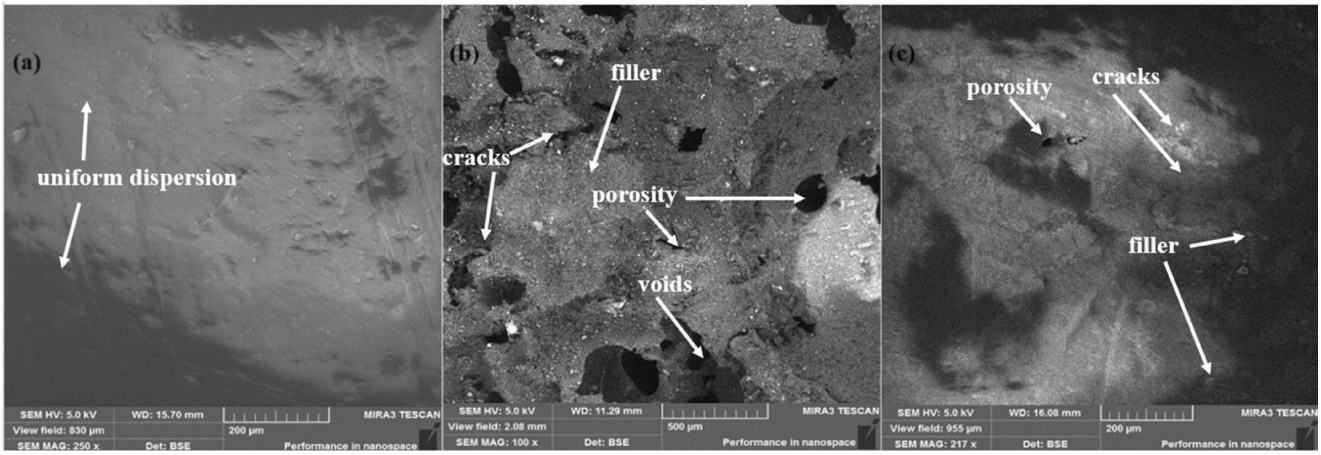

FIGURE 5 | SEM images of samples: (a) "13i," (b) "15i," (c) "17 m."

stretching interactions, 1537 cm^{-1} for C—N (II) band stretching vibrations, 1596 cm^{-1} for aromatic C═C/C—C stretching interactions, and 2967 cm^{-1} for weakly C—H asymmetric stretching vibrations. Throughout both FTIR analyses, variations in band intensity were observed, indicating changes in permeability for specific vibrational modes within the composite material.

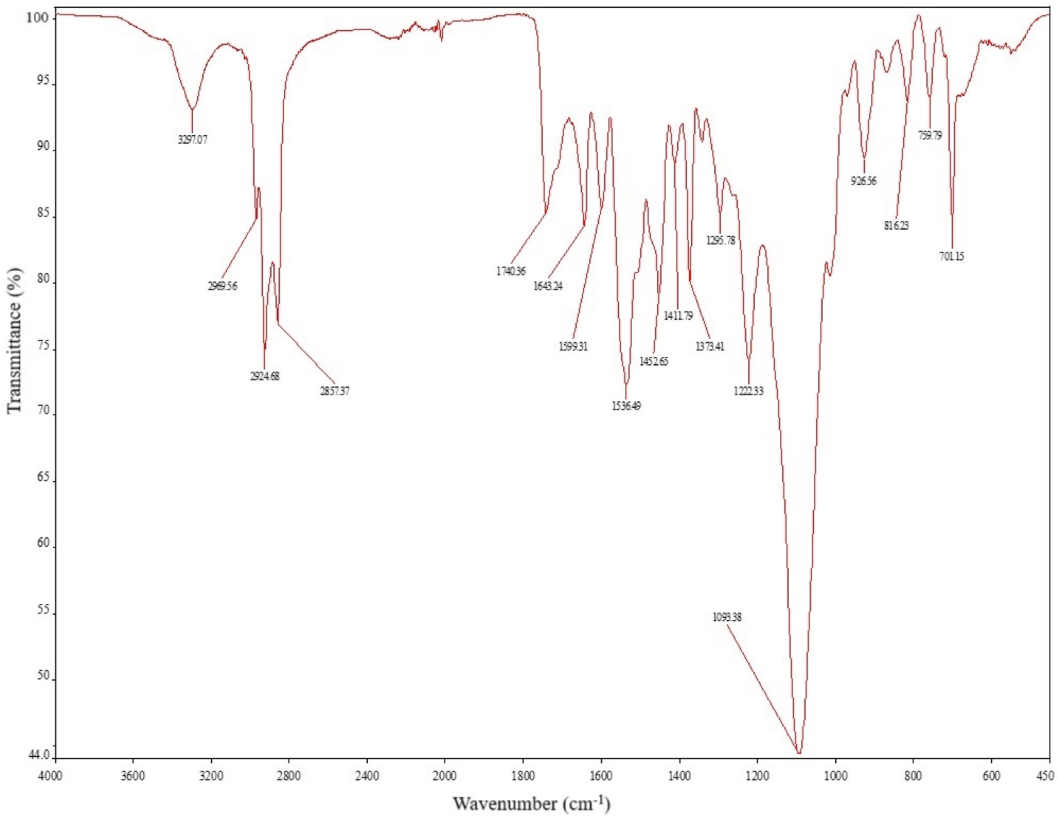

FIGURE 6 | FTIR spectra of the "1o" sample.

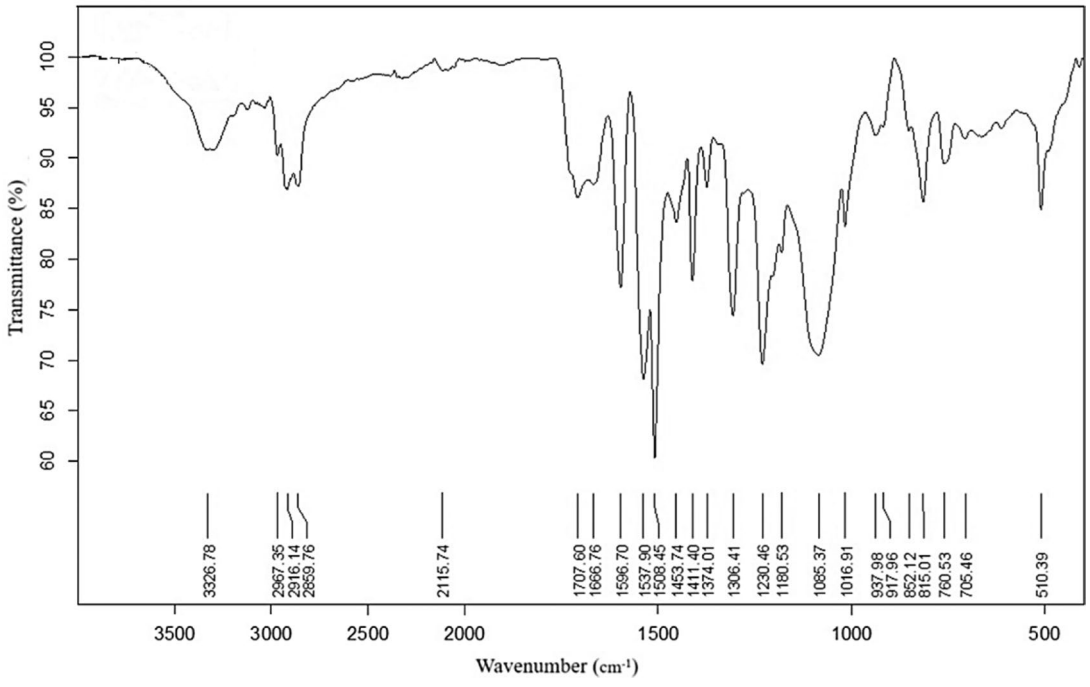

FIGURE 7 | FTIR spectra of sample '1i'.

3.4 | Thermal Conductivity and Corrosion Test Results

The thermal conductivity coefficient (λ) of thermal insulation materials exhibits variability. For instance, 0.035–0.040 W/m·K for expanded polystyrene, 0.030–0.040 W/m·K for extruded polystyrene, 0.035–0.050 W/m·K for rock wool and glass wool, and for heat insulation plaster, 0.055–0.100 W/m·K [47, 48]. It is noteworthy that the thermal conduction coefficient varies across different materials, and there exists a general range in

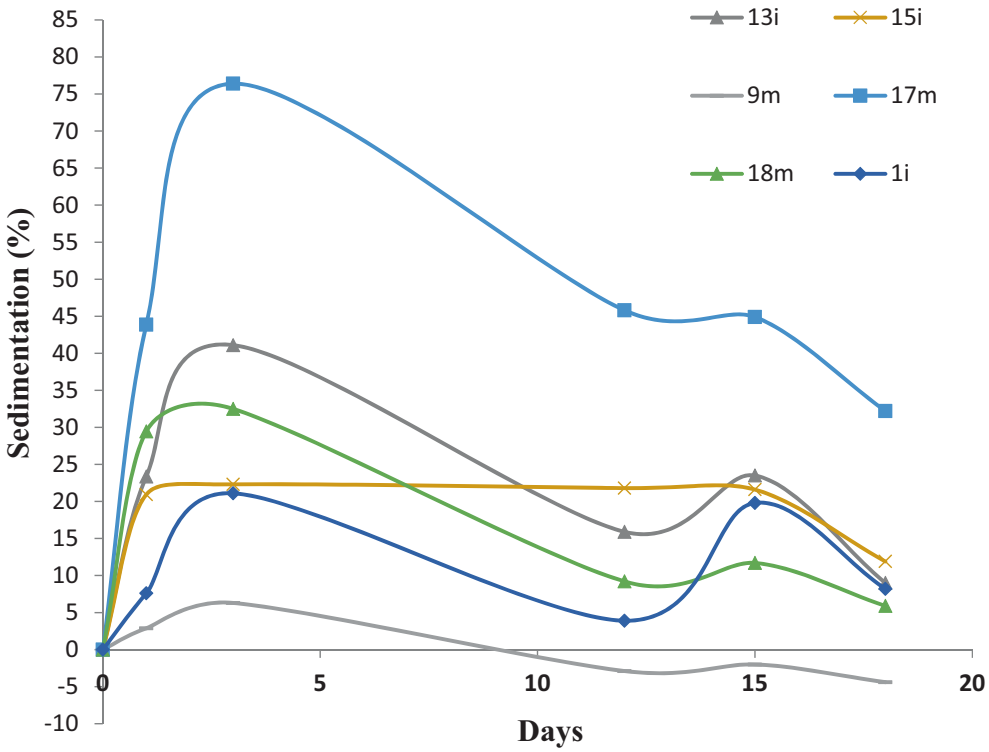

FIGURE 8 | Corrosion analysis graph.

building materials. Within this range, materials with values falling between 0.030 and 0.100 W/m·K are considered suitable for use as insulation materials. The measured thermal conductivity coefficients of the obtained samples are presented in Table 3.

Tests aimed at determining the resistance of industrial building and construction materials, such as metals, concrete, and composites, to corrosion in a significantly shorter time than the corrosion times occurring under normal conditions, employing "corrosion mechanisms," are referred to as corrosion tests [49, 50]. In these tests, the materials undergo exposure to specific environmental conditions, typically manipulating one or a few parameters (such as salt spray, UV radiation, sprinkling, humidity), and the material's durability is assessed [51].

Upon examining the corrosion graph in Figure 8, the following conclusions can be drawn:

- Sample 1i (salt clay waste): Salt clay waste has enhanced the strength of the polyurethane matrix by strengthening hydrogen bonds. Based on the trend in the graph, the corrosion effect on sample 1i appears to be moderate, stabilizing around 20%–30% over time. This suggests that salt clay provides a partially protective effect, although its hygroscopic nature prevents complete inhibition of corrosion in the long term.
- Sample 9 m (salt clay waste—ulexite): The addition of ulexite has increased compressive strength and hardness. Boron compounds are known to improve structural durability. In sample 9 m, the sedimentation rate remained lower than that of the other samples (maximum of 20%). This indicates that ulexite acts as an effective protective barrier, partially balancing the hygroscopic properties within the material.
- Sample 13i (salt clay waste—ulexite—colemanite): The addition of colemanite significantly increased compressive strength (400%–500%). The rigid and crystalline structure of colemanite enhanced the material's durability. Sample 13i showed moderate resistance to corrosion effects. Colemanite appears to have delayed the onset of corrosion, but it did not completely prevent it over the long term.
- Sample 15i (salt clay waste—ulexite—colemanite—Kırka clay waste): The addition of Kırka clay waste increased the density of the material and improved its strength properties. In the corrosion graph of sample 15i, the sedimentation rate remained stable at a certain level. The use of Kırka clay as a filler may have contributed to increased density, providing partial resistance to corrosion.
- Sample 17 m (salt clay waste—ulexite—colemanite—Kırka clay waste—tincal—coal ash): The addition of fly ash increased the porosity of the material, which in turn slightly enhanced the compressive strength. In sample 17 m, the corrosion rate initially rose to 85% before decreasing. This high initial corrosion was likely due to the porous structure and hygroscopic properties of fly ash, suggesting that the material was more susceptible to corrosion upon contact with moisture.
- Sample 18 m (salt clay waste—ulexite—colemanite—Kırka clay waste—tincal—coal ash (fly ash)-ulexite clay (70 wt.% water)): The addition of ulexite clay increased the material's strength and hardness. In sample 18 m, the corrosion effect initially increased but later stabilized at around 40%. This indicates that the material initially interacted with moisture, but this interaction stabilized over time.

In conclusion, it can be stated that sample 17 m exhibited the highest corrosion rate, which can be attributed to the porous structure

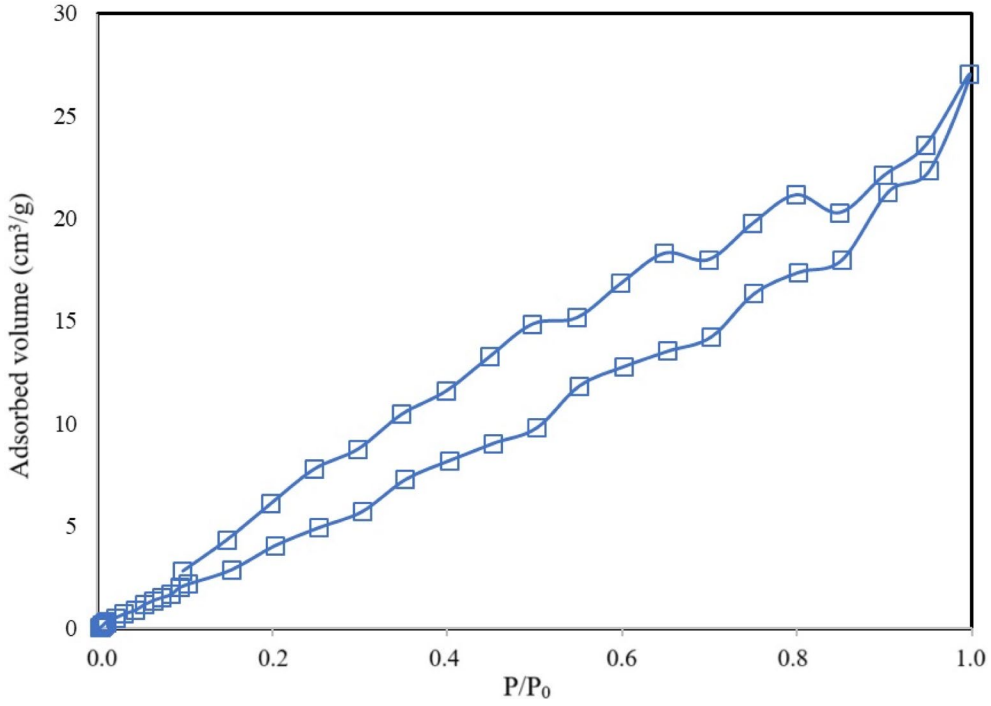

FIGURE 9 | Adsorbed volume vs. high relative pressure (P/P_0) graph of sample "1i."

of the fly ash it contains. Porous structures allow water to penetrate the material, increasing corrosion. In contrast, sample 9m demonstrated the best performance against corrosion. Ulexite may have acted as a protective barrier within the polyurethane matrix, reducing the material's susceptibility to moisture and corrosion. Boron compounds such as colemanite and tincal provided some degree of corrosion protection, though they did not completely prevent it over the long term.

3.5 | Brunauer-Emmett-Teller (BET) Surface Area Analysis Results

Surface area analysis serves the purpose of determining pore size and distribution in porous powder or solid samples, utilizing the physical adsorption method at high and low pressures. The analysis devices used in this context trace back to the theory of Brunauer, Emmett, and Teller, particularly during calculations. The analysis was performed using a Quantachrome Nova Touch LX4 BET device. The Brunauer-Emmett-Teller (BET) analysis result for sample "1i" is presented in Figure 9. The isotherm observed here is close to a Type IV region isotherm. This indicates that mesopores are present in the initial region of sample "1i," and the isotherm appears to follow a path parallel to the pressure axis near the saturation pressure. It is believed that inadequate mixing of the "1i" sample, resulting in incomplete gas release before the molding process, may have caused this condition. Additionally, the presence of a hysteresis loop indicates that the material has a distinct pore structure capable of adsorbing gases. The effect of salt clay on this structure, along with the polyurethane matrix, may have enhanced the composite's surface properties, influencing its adsorption capacity and porosity. This porous structure could potentially enhance the composite's applicability in various fields, such as catalysis or filtration.

3.6 | Machine Learning Results

The effect of each filler on pure polyurethane was analyzed using artificial intelligence and machine learning techniques in Python. The resulting graphs are presented in Figure 10.

Upon examining Figure 10, the effects of each filler on the polyol can be summarized as follows:

-Salt clay waste: Salt clay typically contains sodium and magnesium salts, which provide an inorganic structure. The dispersion of salt clay within the polyurethane matrix significantly increased compressive strength (approximately 300%–500%). This improvement is attributed to salt clay particles filling the porous structure of polyurethane, leading to a more compact and durable material. The salts also strengthen hydrogen bonds within the polyurethane, contributing to an increase in hardness (25%–40%). However, due to the hygroscopic nature of salt clay, it should be noted that such a filler may have adverse effects when exposed to moisture.

-Ulexite ($NaCaB_5O_9{\cdot}8H_2O$): Ulexite is a boron-containing mineral that includes sodium, calcium, and boron compounds. When incorporated into the polyurethane matrix, the rigid structure of boron compounds led to an increase in compressive strength (approximately 250–350%). This is due to boron's ability to enhance structural durability. Boron minerals also form a physical barrier within the polyurethane, making the material more compact. Additionally, boron compounds partially interact with polyurethane chemically, increasing cross-linking and thus enhancing hardness by up to 30%. These interactions also provide additional properties, such as improved fire resistance.

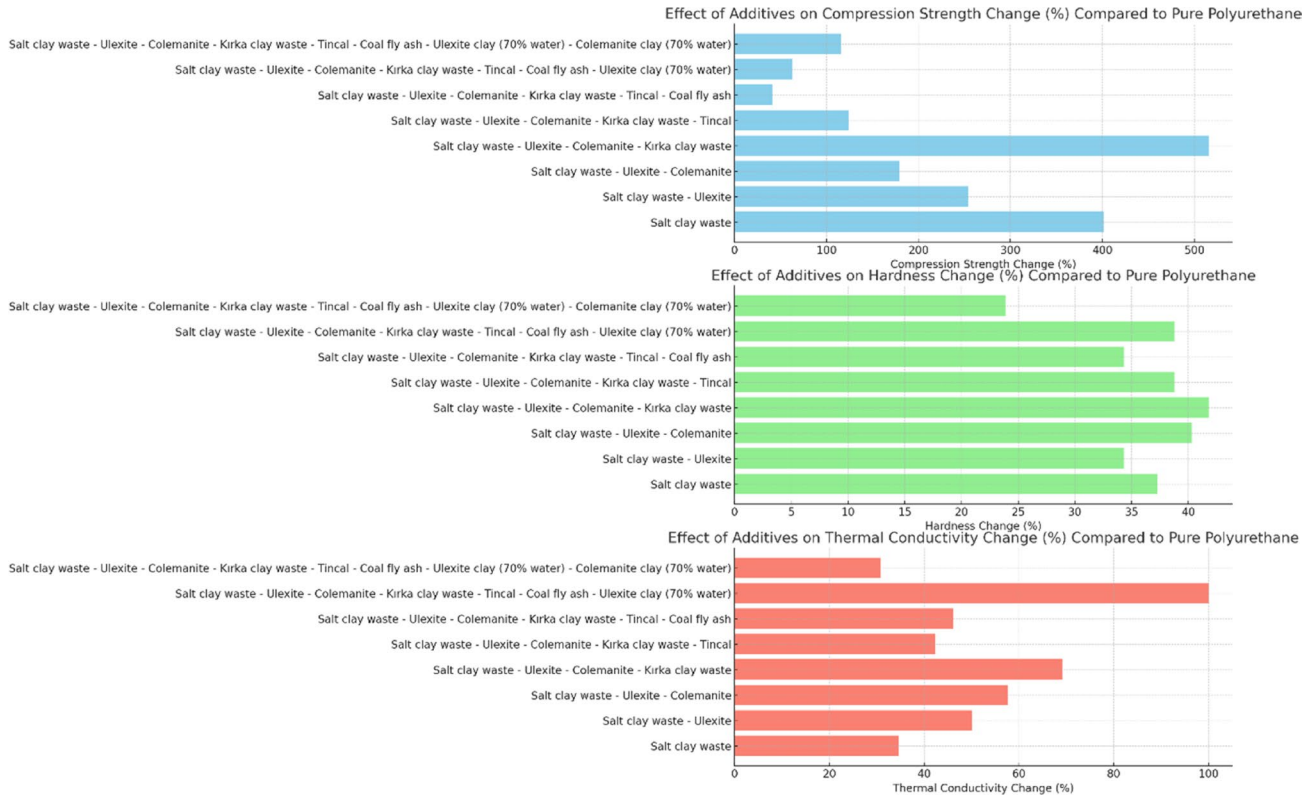

FIGURE 10 | Percentage effects of fillers on compressive strength, hardness, and thermal conductivity.

-Colemanite ($Ca_2B_6O_{11}\cdot 5H_2O$): Colemanite contains calcium and boron components and has a rigid structure. It significantly increased compressive strength (400%–500%) due to its hardness and crystalline structure, which enhanced the compressive resistance of the polyurethane. Adding colemanite resulted in a more homogeneous and rigid composite. Colemanite interacts with the isocyanate groups in polyurethane, increasing the cross-linking rate, which contributes to improved hardness (35%–40%).

-Kırka clay waste: Kırka clay waste contains silicate and carbonate minerals. The addition of Kırka clay increased compressive strength (300%–450%). This improvement is due to the clay being used as a filler, which increases the material's density. The clay minerals act as a physical filler within the polyurethane, with limited chemical bonding to the matrix. However, due to their water-retaining properties, the long-term absorption of moisture could negatively impact performance.

-Tincal ($Na_2B_4O_7\cdot 10H_2O$): Tincal, also known as borax, is a sodium borate compound known for its high boron content. The addition of borax led to an increase in both compressive strength and hardness. The crystalline structure of borax distributed homogeneously within the polyurethane matrix, enhancing compressive strength. Borax can chemically interact with isocyanate groups in polyurethane, providing cross-linking, which supports the hardening of the material and adds properties such as improved fire resistance.

-Coal ash (fly ash): Fly ash, containing silica and alumina, is a low-density and porous material. Its addition provided a significant increase in compressive strength but had a more limited effect on hardness. The low density and porosity of fly ash, when used as a filler in polyurethane, contributed to improved mechanical strength. Chemically, fly ash showed limited interaction with polyurethane. Its porous nature, however, gives it a high potential for moisture retention, which could negatively affect the long-term durability of the material.

The effect of each filler on the parameters can be summarized as follows: Inorganic minerals such as colemanite, ulexite, and Kırka clay waste have increased the compressive strength of polyurethane, resulting in a stronger and more compact structure. The addition of these minerals filled the porous structure of the polyurethane, yielding a denser material. Boron-based fillers (e.g., colemanite and tincal) significantly increased hardness by enhancing the cross-linking rate of the polyurethane. This contributed to the material becoming more durable and rigid. The fillers generally increased thermal conductivity, which reduced the insulation properties of the composite. Specifically, the addition of fly ash and other minerals led to higher heat transfer within the material.

Using artificial intelligence, different machine learning models were applied with Python, and the results are presented in graphical form in Figure 11.

After comparing the models, the next step involved applying supervised learning within artificial intelligence and machine learning to model the relationship between independent variables (input parameters) and dependent variables (output) in

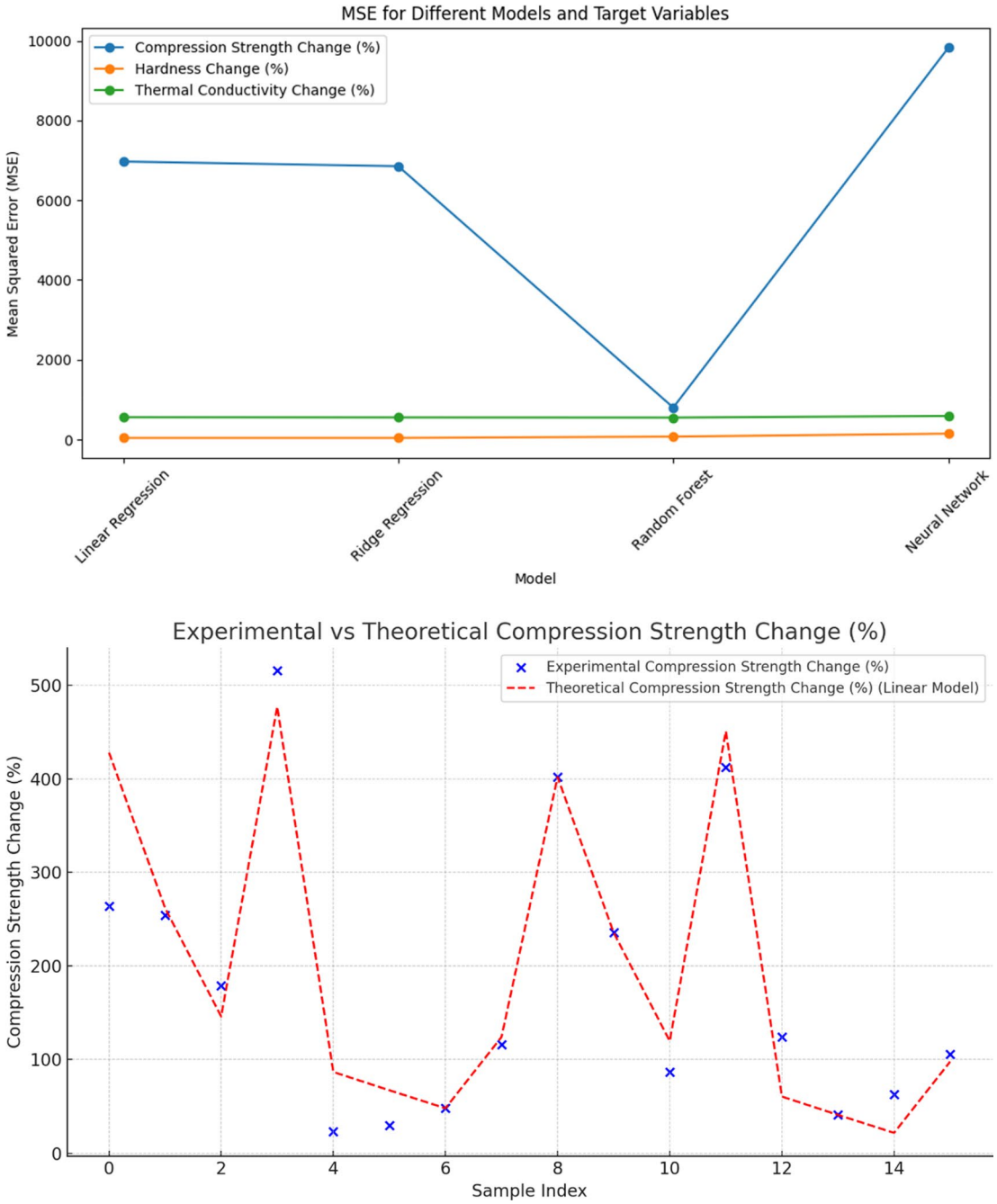

FIGURE 11 | Comparison of machine learning models. Comparison of theoretical and experimental data for compressive strength.

a linear manner. The equations obtained for each variable are shown below as Equation (1), Equation (2), and Equation (3):

$$\begin{aligned}&\text{Compression strength change (\%)}\\&=128.4170+1.5078\times\text{polymer amount (g)}\\&+2.5654\times\text{waste amount (g)}\\&-5.3339\times\text{waste combination encoded}\end{aligned}\tag{1}$$

- Constant term (128.4170): This value represents the percentage change in compressive strength when the effect of all independent variables is zero (i.e., for pure polyurethane).
- Polymer amount (1.5078): The positive coefficient indicates that increasing the polymer amount has a positive effect on compressive strength.
- Waste amount (2.5654): The positive coefficient suggests that an increase in waste amount can enhance compressive strength.
- Waste combination encoded (−5.3339): This coefficient represents a factor affecting compressive strength for a particular sample code (e.g., 1o, 1i). The negative value suggests that these combinations may have a negative impact on compressive strength.

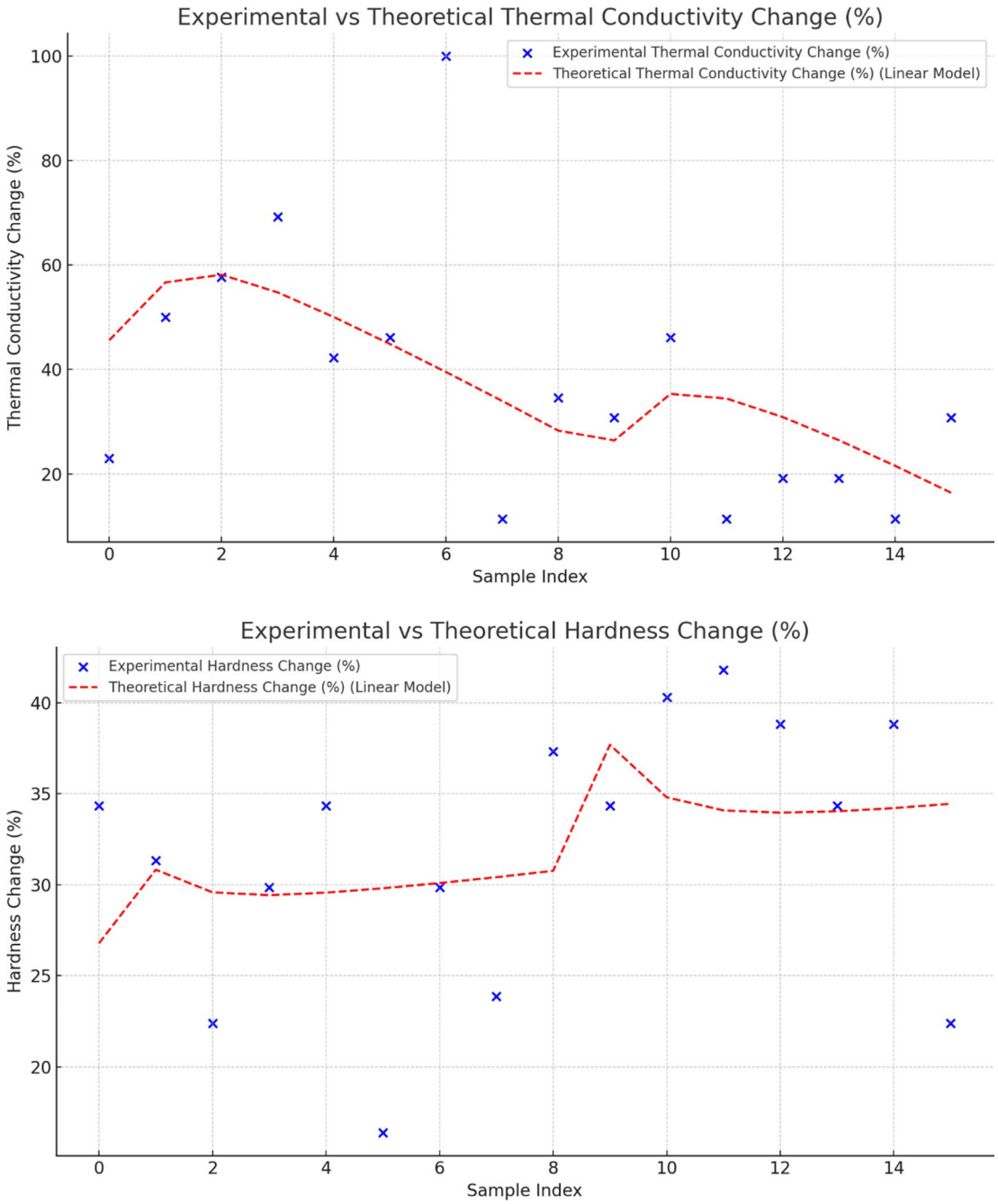

FIGURE 12 | Comparison of theoretical and experimental data for thermal conductivity. Comparison of theoretical and experimental data for hardness.

The comparison of experimental and theoretical data derived from the equation obtained for compressive strength is shown in Figure 12. It can be generally stated that the obtained equation successfully predicts the experimental results.

$$\begin{aligned}&\text{Thermal conductivity change (\%)}\\&= 140.7504 - 1.2684 \times \text{polymer amount (g)}\\&- 0.5904 \times \text{waste amount (g)}\\&- 5.8953 \times \text{waste combination encoded}\end{aligned} \tag{2}$$

- Constant term (140.7504): Represents the baseline level of thermal conductivity change.
- Polymer amount (−1.2684): The negative coefficient indicates that increasing the polymer amount has a reducing effect on thermal conductivity.
- Waste amount (−0.5904): The negative coefficient suggests that an increase in waste amount also has a reducing effect on thermal conductivity.
- Waste combination encoded (−5.8953): Indicates that the waste combination has a negative impact on thermal conductivity.

The comparison of experimental and theoretical data derived from the equation obtained for thermal conductivity is shown in

Figure 11. It can generally be stated that the obtained equation successfully predicts the experimental results.

$$\begin{aligned}&\text{Hardness change (\%)}\\&=27.8171-0.0138\times\text{polymer amount (g)}\\&+0.1316\times\text{waste amount (g)}+0.4033\\&\times\text{waste combination encoded}\end{aligned}\tag{3}$$

- Constant term (27.8171): Represents the baseline level of hardness change.
- Polymer amount (−0.0138): There is a very slight negative effect of increasing the polymer amount on hardness.
- Waste amount (0.1316): The positive coefficient indicates that increasing the waste amount has a positive effect on hardness.
- Waste combination encoded (0.4033): The waste combination has a positive impact on hardness.

The comparison of experimental and theoretical data derived from the equation obtained for hardness is shown in Figure 12. It can generally be stated that the obtained equation has moderate success in predicting the experimental results.

4 | Conclusions

This study successfully developed polyurethane-based composites incorporating salt clay, ulexite, colemanite, and various industrial waste materials, demonstrating substantial improvements in mechanical and thermal properties. By effectively utilizing waste materials, the research not only enhances material performance but also promotes sustainable waste management practices. The composite formulations led to remarkable increases in compressive strength, hardness, and thermal insulation capabilities, indicating their potential suitability for diverse industrial applications.

The incorporation of salt clay proved to be particularly effective, delivering a 300%–500% increase in compressive strength and a 25%–40% improvement in hardness. Similarly, ulexite and colemanite fillers contributed significantly to mechanical enhancement, while fly ash provided additional compressive strength benefits. The combined effect of these fillers resulted in composites with thermal conductivity values ranging between 0.030 and 0.050 W/m·K, making them excellent candidates for insulation materials and lightweight, low-load structural components.

A key innovation of this research was the integration of machine learning techniques, which allowed accurate prediction of composite performance based on experimental data. Among the models tested, random forest and neural networks achieved superior predictive accuracy for compressive strength, hardness, and thermal conductivity, with low mean squared error values. These findings underscore the utility of data-driven approaches in optimizing material design and performance without relying solely on traditional experimental methods.

The industrial relevance of the developed composites is clear, as they combine improved mechanical and thermal performance with sustainable resource use. Potential applications include thermal insulation in buildings, lightweight structural elements, and components exposed to moderate mechanical loads. The positive results also suggest a promising avenue for utilizing other types of industrial wastes, further broadening the scope of eco-friendly material development.

Future work will focus on evaluating the long-term durability of these composites under real-world service conditions, including exposure to environmental factors such as moisture, temperature cycling, and chemical agents. Additionally, expanding the machine learning framework to incorporate more complex models and larger datasets may further enhance the predictive capabilities and optimization of composite formulations. Overall, this study lays a strong foundation for advancing sustainable composite materials and integrating artificial intelligence into materials research.

Author Contributions

Mustafa Dağ: writing, acquisition of data, analysis of data, approval of the version of the manuscript to be published, review and editing. **Ercan Aydoğmuş:** writing, acquisition of data, analysis of data, approval of the version of the manuscript to be published, review and editing. **Hasan Arslanoğlu:** writing, revising the manuscript critically for important intellectual content, approval of the version of the manuscript to be published, review and editing. **Zehra Gülten Yalçin:** writing, revising the manuscript critically for important intellectual content, approval of the version of the manuscript to be published. **Semahat Barlak:** writing, revising the manuscript critically for important intellectual content, approval of the version of the manuscript to be published.

Conflicts of Interest

The authors declare no conflicts of interest.

Data Availability Statement

The data that support the findings of this study are available from the corresponding author upon reasonable request.

References

1. P. Rai, J. Lee, R. Brown, and K. K. Kang, "Micro- and Nano-Plastic Pollution: Behavior, Microbial Ecology, and Remediation Technologies," *Journal of Cleaner Production* 291 (2021): 125240.

2. X. Chang, Y. Xue, J. Li, L. Zou, M. Tang, and C. Y. Xue, "Potential Health Impact of Environmental Micro- and Nanoplastics Pollution," *Journal of Applied Toxicology* 40, no. 1 (2019): 4–15, https://doi.org/10.1002/jat.3915.

3. M. Allouzi, D. Tang, K. Chew, et al., "Micro(Nano) Plastic Pollution: The Ecological Influence on Soil-Plant System and Human Health," *Science of the Total Environment* 788 (2021): 147815.

4. P. Praus, "Photoreforming for Microplastics Recycling: A Critical Review," *Journal of Environmental Chemical Engineering* 12, no. 3 (2024): 112525, https://doi.org/10.1016/j.jece.2024.112525.

5. M. E. Grigore, "Methods of Recycling, Properties and Applications of Recycled Thermoplastic Polymers," *Recycling (Basel)* 2, no. 4 (2017): 1–10, https://doi.org/10.3390/recycling2040024.

6. D. G. Hayes and M. J. Dumont, "Polymeric Products Derived From Industrial Oils for Paints, Coatings, and Other Applications," in *Industrial*

Oil Crops, ed. F. Shahidi (AOCS Press, 2016), 43–73, https://doi.org/10.1016/B978-1-893997-98-1.00003-8.

7. M. S. Khan, M. Sohail, N. S. Khattak, and M. Sayed, "Industrial Ceramic Waste in Pakistan, Valuable Material for Possible Applications," *Journal of Cleaner Production* 139 (2016): 1520–1528, https://doi.org/10.1016/j.jclepro.2016.08.131.

8. O. Das, K. Babu, V. Shanmugam, et al., "Natural and Industrial Wastes for Sustainable and Renewable Polymer Composites," *Renewable and Sustainable Energy Reviews* 158 (2022): 112054, https://doi.org/10.1016/j.rser.2021.112054.

9. A. Agrawal, A. Purohit, G. Gupta, S. K. Nayak, P. R. Pati, and A. Satapathy, "Utilization of Industrial Waste as Filler Material in the Development of Polymer Composites," in *Composites: Modeling and Manufacturing* (CRC Press, 2024), 66–85.

10. S. Mohanty, N. R. Dutta, H. Jena, P. Pradhan, A. Purohit, and P. R. Pati, "Enhancing Mechanical Properties of Basalt Fibre Composites With Clamshell Waste From Sea Bed," *Journal of Solid Waste Technology and Management* 50, no. 3 (2024): 532–542, https://doi.org/10.5276/JSWTM/ISWMAW/503/2024.532.

11. A. Purohit and A. Satapathy, "Development and Characterization of Epoxy-Based Composites Filled With Linz-Donawitz Sludge," *Journal of Composite Materials* 51, no. 7 (2017): 899–911, https://doi.org/10.1177/0021998316656478.

12. A. Purohit, P. Pradhan, S. Palanimuthu, A. Kumar, and P. K. Chauhan, "Mechanical and Tribological Characteristics of Glass Fiber and Rice Stubble-Filled Epoxy-LD Sludge Hybrid Composites," *Journal of Elastomers and Plastics* 57, no. 1 (2024): 113–131, https://doi.org/10.1177/00952443241305709.

13. R. Das and C. Bhattacharjee, "Green Composites, the Next-Generation Sustainable Composite Materials: Specific Features and Applications," in *Green Sustainable Process for Chemical and Environmental Engineering and Science* (Elsevier, 2022), 55–70, https://doi.org/10.1016/B978-0-323-99643-3.00018-8.

14. M. H. Demirel and E. Aydoğmuş, "Waste Polyurethane Reinforced Polyester Composite, Production and Characterization," *J Turk Chem Soc A Chem* 9, no. 2 (2022): 443–452, https://doi.org/10.18596/JOTCSA.937332.

15. A. D. La Rosa, G. Recca, J. Summerscales, A. Latteri, G. Cozzo, and G. Cicala, "Bio-Based Versus Traditional Polymer Composites. A Life Cycle Assessment Perspective," *Journal of Cleaner Production* 74 (2014): 135–144, https://doi.org/10.1016/j.jclepro.2014.03.017.

16. E. Aydoğmuş, "Biohybrid Nanocomposite Production and Characterization by RSM Investigation of Thermal Decomposition Kinetics With ANN," *Biomass Conversion and Biorefinery* 12, no. 10 (2022): 4799–4816, https://doi.org/10.1007/s13399-022-02403-6.

17. D. J. Sikkema, "Chapter 4: Rigid-Chain Polymers: Aromatic Polyamides, Heterocyclic Rigid Rod Polymers, and Polyesters," in *Advanced Industrial and Engineering Polymer Research* (Elsevier, 2022), https://doi.org/10.1016/j.aiepr.2022.03.003.

18. R. Kumar, R. Singh, and M. S. J. Hashmi, "Polymer-Ceramic Composites: A State of Art Review and Future Applications," *Advances in Materials and Processing Technologies* 8, no. 1 (2022): 895–908, https://doi.org/10.1080/2374068X.2020.1835013.

19. R. Yang, G. Xu, W. Tao, Q. Wang, and Y. Tang, "Recycled Polymer: Green Roads for Polyester Plastics," *Green Carbon* 2, no. 1 (2024): 1–11, https://doi.org/10.1016/j.greenca.2024.01.004.

20. N. Zari, M. Raji, H. El Mghari, R. Bouhfid, and A. E. K. Qaiss, "Nanoclay and Polymer-Based Nanocomposites: Materials for Energy Efficiency," in *Polymer-Based Nanocomposites for Energy and Environmental Applications* (Woodhead Publishing, 2018), 75–103, https://doi.org/10.1016/B978-0-08-102262-7.00003-9.

21. M. F. Sonnenschein, V. V. Ginzburg, K. S. Schiller, and B. L. Wendt, "Design, Polymerization, and Properties of High Performance Thermoplastic Polyurethane Elastomers From Seed-Oil Derived Soft Segments," *Polymer (Guildf)* 54, no. 4 (2013): 1350–1360, https://doi.org/10.1016/j.polymer.2012.12.077.

22. A. Nakajima, H. Hamada, and S. Hayashi, "Structure and Some Physical Properties of Polyvinyl Chloride Polymerized at Different Temperatures," *Die Makromolekulare Chemie* 95, no. 1 (1966): 40–51, https://doi.org/10.1002/MACP.1966.020950103.

23. D. A. Şerban, G. Weber, L. Marşavina, V. V. Silberschmidt, and W. Hufenbach, "Tensile Properties of Semi-Crystalline Thermoplastic Polymers: Effects of Temperature and Strain Rates," *Polymer Testing* 32, no. 2 (2013): 413–425, https://doi.org/10.1016/j.polymertesting.2012.12.002.

24. H. Jena, P. Pradhan, and A. Purohit, "Dielectric Properties, Thermal Analysis, and Conductivity Studies of Biodegradable and Biocompatible Polymer Nanocomposites," in *Biodegradable and Biocompatible Polymer Nanocomposites: Processing, Characterization, and Applications* (Elsevier, 2023), 113–140, https://doi.org/10.1016/B978-0-323-91696-7.00011-8.

25. F. Zia, K. M. Zia, M. Zuber, S. Kamal, and N. Aslam, "Starch Based Polyurethanes: A Critical Review Updating Recent Literature," *Carbohydrate Polymers* 134 (2015): 784–798, https://doi.org/10.1016/j.carbpol.2015.08.034.

26. N. Karak, "Vegetable Oil-Based Polyurethanes," in *Vegetable Oil-Based Polymers* (Elsevier, 2012), 146–179, https://doi.org/10.1533/9780857097149.146.

27. D. K. Chattopadhyay and D. C. Webster, "Thermal Stability and Flame Retardancy of Polyurethanes," *Progress in Polymer Science* 34, no. 10 (2009): 1068–1133, https://doi.org/10.1016/j.progpolymsci.2009.06.002.

28. J. O. Akindoyo, M. D. H. Beg, S. Ghazali, M. R. Islam, N. Jeyaratnam, and A. R. Yuvaraj, "Polyurethane Types, Synthesis and Applications-A Review," *RSC Advances* 6, no. 115 (2016): 114453–114482, https://doi.org/10.1039/C6RA14525F.

29. M. Kato, H. Okamoto, N. Hasegawa, A. Tsukigase, and A. Usuki, "Preparation and Properties of Polyethylene-Clay Hybrids," *Polymer Engineering and Science* 43, no. 6 (2003): 1312–1316, https://doi.org/10.1002/PEN.10111.

30. M. Zuber, K. M. Zia, S. Mahboob, M. Hassan, and I. A. Bhatti, "Synthesis of Chitin-Bentonite Clay Based Polyurethane Bio-Nanocomposites," *International Journal of Biological Macromolecules* 47, no. 2 (2010): 196–200, https://doi.org/10.1016/j.ijbiomac.2010.04.022.

31. S. Liuzzi, C. Rubino, and P. Stefanizzi, "Use of Clay and Olive Pruning Waste for Building Materials With High Hygrothermal Performances," *Energy Procedia* 126 (2017): 234–241, https://doi.org/10.1016/j.egypro.2017.08.145.

32. C. Yanen and D. Mustafa, "Investigation of Thermophysical Properties of Colemanite, Ulexite, and Tincal Reinforced Polyester Composites," *EJOSAT* 36 (2022): 155–159, https://doi.org/10.31590/ejosat.1008386.

33. G. Guzel, O. Sivrikaya, and H. Deveci, "The Use of Colemanite and Ulexite as Novel Fillers in Epoxy Composites: Influences on Thermal and Physico-Mechanical Properties," *Composites Part B: Engineering* 100 (2016): 1–9, https://doi.org/10.1016/j.compositesb.2016.06.054.

34. İ. Bilici, B. Aygün, C. U. Deniz, B. Öz, M. I. Sayyed, and A. Karabulut, "Fabrication of Novel Neutron Shielding Materials: Polypropylene Composites Containing Colemanite, Tincal and Ulexite," *Progress in Nuclear Energy* 141 (2021): 103954, https://doi.org/10.1016/j.pnucene.2021.103954.

35. J. Sim, Y. Kang, B. J. Kim, Y. H. Park, and Y. C. Lee, "Preparation of Fly Ash/Epoxy Composites and Its Effects on Mechanical Properties," *Polymers (Basel)* 12, no. 1 (2020): 1–12, https://doi.org/10.3390/polym12010079.

36. I. Goodfellow, Y. Bengio, and A. Courville, *Deep Learning* (MIT Press, 2016), https://doi.org/10.4258/hir.2016.22.4.351.

37. J. Schmidhuber, "Deep Learning in Neural Networks: An Overview," *Neural Networks* 61 (2015): 85–117.

38. Y. LeCun, Y. Bengio, and G. Hinton, "Deep Learning," *Nature* 521, no. 7553 (2015): 436–444, https://doi.org/10.1038/nature14539.

39. P. Pradhan, A. Purohit, H. Jena, J. Singh, and B. B. Sahoo, "Effects of Spherical Fillers Reinforcement on the Efficacy of Thermal Conductivity in Epoxy and Polyester Matrices: Experimental Validation and Prediction Using Finite Element Method," *Journal of Vinyl & Additive Technology* 31, no. 1 (2025): 109–120, https://doi.org/10.1002/vnl.22159.

40. A. Mahajan, S. Gairola, I. Singh, and N. Arora, "Optimized Random Forest Model for Predicting Flexural Properties of Sustainable Composites," *Polymer Composites* 45, no. 12 (2024): 10700–10710, https://doi.org/10.1002/pc.28501.

41. C. Joo, H. Park, H. Kwon, et al., "Machine Learning Approach to Predict Physical Properties of Polypropylene Composites: Application of MLR, DNN, and Random Forest to Industrial Data," *Polymers (Basel)* 14, no. 17 (2022): 3500, https://doi.org/10.3390/polym14173500.

42. X. Gao, L. Wang, and L. Yao, "Porosity Prediction of Ceramic Matrix Composites Based on Random Forest," 768, no. 5 (2020).

43. C. C. Nwobi-Okoye and C. U. Uzochukwu, "RSM and ANN Modeling for Production of Al 6351/Egg Shell Reinforced Composite: Multi Objective Optimization Using Genetic Algorithm," *Materials Today Communications* 22 (2020): 100674, https://doi.org/10.1016/j.mtcomm.2019.100674.

44. B. Vural Kök, E. Aydoğmuş, M. Yilmaz, and M. Akpolat, "Investigation on the Properties of New Palm-Oil-Based Polyurethane Modified Bitumen," *Construction and Building Materials* 289 (2021): 123152, https://doi.org/10.1016/j.conbuildmat.2021.123152.

45. W. Q. Qu, Y. R. Xia, L. J. Jiang, L. W. Zhang, and Z. S. Hou, "Synthesis and Characterization of a New Biodegradable Polyurethanes With Good Mechanical Properties," *Chinese Chemical Letters* 27, no. 1 (2016): 135–138, https://doi.org/10.1016/j.cclet.2015.07.018.

46. K. Ashida, "Chemistry and Technology," in *Polyurethane and Related Foams* (Elsevier, 2006).

47. B. Abu-Jdayil, A. H. Mourad, W. Hittini, M. Hassan, and S. Hameedi, "Traditional, State-Of-The-Art and Renewable Thermal Building Insulation Materials: An Overview," *Construction and Building Materials* 214 (2019): 709–735, https://doi.org/10.1016/j.conbuildmat.2019.04.102.

48. Y. X. Fu, Z. X. He, D. C. Mo, and S. S. Lu, "Thermal Conductivity Enhancement With Different Fillers for Epoxy Resin Adhesives," *Applied Thermal Engineering* 66, no. 1–2 (2014): 493–498, https://doi.org/10.1016/j.applthermaleng.2014.02.044.

49. G. Li, L. Chen, Y. An, M. Gao, H. Zhou, and J. Chen, "Investigating the Effect of Polytetrafluoroethylene on the Tribological Properties and Corrosion Resistance of Epoxy/Hydroxylated Hexagonal Boron Nitride Composite Coatings," *Corrosion Science* 210 (2023): 110820, https://doi.org/10.1016/j.corsci.2022.110820.

50. I. B. Obot, M. M. Solomon, S. A. Umoren, et al., "Progress in the Development of Sour Corrosion Inhibitors: Past, Present, and Future Perspectives," *Journal of Industrial and Engineering Chemistry* 79 (2019): 1–18, https://doi.org/10.1016/j.jiec.2019.06.046.

51. Y. Sun, S. Yuan, W. Fan, et al., "A Smart Composite Coating With Photothermal Response, Anti-UV and Anti-Corrosion Properties," *Chemical Engineering Journal* 452 (2023): 138983, https://doi.org/10.1016/j.cej.2022.138983.